Adaptive Power Control Strategy for Smart Droop-Based Grid-Connected Inverters

Nabil Mohammed, *Member, IEEE*, and Mihai Ciobotaru, *Senior Member, IEEE*

***Abstract*—Grid-connected inverters play an important role in the integration of renewable energy sources such as solar and wind. However, due to the unneglectable grid impedance value seen by the inverters at the point of common coupling (PCC), especially in the weaks and resistive low voltage distribution networks, there is an inherent strong coupling between active and reactive power flow. This power coupling causes significant power quality problems including 1) voltage fluctuation of the common AC bus resulted from high penetration of intermittent renewable generation systems, 2) non-optimal control of neither power flow nor power factor of the delivered power by inverters to the common AC bus, and 3) unintended/uncompensated transmission losses, where the flow of active power through the transmission/distribution lines will cause unintended reverse reactive power flow from the grid-side and vice versa with the reactive power flow. To solve these issues, this paper proposes an adaptive mechanism for droop-based grid-connected inverters to decouple the power flow by compensating the associated unintended active and reactive power losses flowing through the transmission line (or any desired segment of it). This control strategy relies on modifying the power command provided to the frequency and voltage droop loops by considering the effects of both the transmission line resistance and inductance components on the power flow between the inverter and the grid. It uses only the local current and voltage measurements to first perform an online estimation of the transmission line resistance and inductance and then to calculate the proposed adaptive power terms. The performance of the proposed control is validated in MATLAB/Simulink and HIL experiment for a 350 kW droop-based grid-connected inverter system. The proposed control strategy can be utilized to provide ancillary services to the grid such as accurate frequency and voltage support at the location of interest.**

***Index Terms*—Adaptive droop control, decoupling power flow, impedance estimation, inverters, transmission loss compensation.**

I. Introduction

THE CURRENT significant changes in the electric power systems are driving the conventional systems towards power-electronics-based power systems. These latter systems allow for greater integration of sustainable energy sources, where grid-connected inverters play an important and direct part in such distributed generation technologies [1]. They permit the integration of renewable systems to different voltage levels. For example, small-scale systems (e.g., household solar PV systems) are integrated into low voltage distribution networks. On the other hand, large-scale systems (e.g., solar PV and wind farms) can be interfaced to medium voltage. The high-penetration levels of grid-connected inverters present several opportunities and challenges [2].

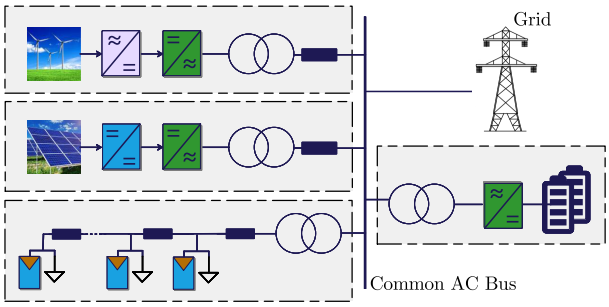

Fig. 1. Integration of renewable energy sources into MV/LV smart grid.

On the one hand, PV/Wind grid-connected inverters have the capability to provide grid support services [3], including reduction of transmission and distribution congestion, line loss reduction [4], peak shaving, voltage regulation [5], frequency regulation [6], and reactive power compensation. The above-mentioned benefits help to increase the PV penetration [7], hence, deferring investments required to upgrade existing infrastructure. Recently, several proposed techniques have verified the effectiveness of using grid-connected inverters for reactive power control, power factor control and voltage regulation at the point of common coupling (PCC) [8]. These ancillary services are achieved by controlling the power flow between the solar PV/wind farm and the AC common bus. Additionally, solar PV inverters can be operated as static synchronous compensators (PV-STATCOMs) night to regulate grid voltage [9].

On the other hand, optimal operation of the grid-connected inverters to provide ancillary services is not a straight forwards. Effects of the unneglectable transmission line impedance, located between the grid-connected inverters (e.g., solar PV-houses and remote PV farms) and the common AC bus, become more clear in MV/LV distribution networks [10] due to their high R/X ratios; see Fig. 1. Major negative impacts of the grid impedance include the instability of grid-connected inverters specially in the presence of varying grid impedance [11] and in weak grid conditions [12], [13].

Manuscript received March 22, 2021; revised August 27, 2021 and October 30, 2021; accepted January 4, 2022. Date of publication January 7, 2022; date of current version April 22, 2022. Paper no. TSG-00439-2021. *(Corresponding author: Nabil Mohammed.)*

The authors are with the School of Engineering, Macquarie University, Sydney, NSW 2109, Australia (e-mail: nabil.mohammed@ieee.org; ciomih@ieee.org).

Color versions of one or more figures in this article are available at https://doi.org/10.1109/TSG.2022.3141265.

Digital Object Identifier 10.1109/TSG.2022.3141265

Furthermore, the grid impedance causes coupling between the active and reactive power flow. For instance, the flow of active power through the distribution lines will cause unintended reactive power flow and vice versa with the reactive power flow. Such coupling prevents precise control of the injected power to the common AC bus (on the grid side), which can be critical in certain applications such as frequency and voltage support. Additionally, the strong coupling between active and reactive power significantly impacts the voltage of the common AC bus under fluctuating renewable power generation. Another drawback of the complex line impedance is the direct effect on the power factor control. For example, a unity power factor is measured at the inverter output once its power references are set to inject only active power. However, the power factor will differ from unity at the common AC bus [14]. This is due to the reverse reactive power flow from the grid side (the common AC bus) towards the distribution line to compensate for the reactive power losses across the line impedance.

Therefore, the negative impacts of the transmission line impedance should be fully mitigated in order to achieve accurate power flow/factor control of the delivered power to the common AC bus corresponding to the desired power references. To overcome the above challenges, the delivered power to the common AC bus has to be regulated, where two main approaches can be distinguished 1) to control the inverter based on the common AC bus measurements by implementing an outer loop controller. The fed control signals of this auxiliary control loop are the measured voltage and current at the PCC, after the transformer and the cable between the inverter (or PV/wind farm) and the PCC. However, the communication infrastructure cost and reliability of this approach are the key disadvantages [15]. Therefore, this approach is not investigated further in this paper, and 2) to control the inverter based on the local measurements and the known feeder and transformer impedances. Then, the delivered active and reactive power to the common AC bus are regulated to their desired references. This goal is achieved through transmission loss compensation. This paper focuses on the second approach.

Several approaches for the flexible power control methods of distributed inverters have been investigated [14], [16], [17]. Authors of [16] verified that optimal power factor control can be achieved if the R/X ratio of the line impedance is measured, hence, deciding the optimal output power of each PV inverter. Additionally, the effects of R/X ratio and SCR in a weak grid have been explored in [17]. Despite the extensive emphasis in the literature on the effects of transmission line impedance on the accurate control of power flow/factor of inverters, there is limited work exploring real-time estimation to mitigate these effects. In [14], an adaptive compensation of reactive power losses has been proposed. It relied on the real-time estimation of the equivalent grid inductance. Even though the proposed technique shows a significant improvement in the mitigation of reactive power fluctuations, there are three main concerns to be addressed and resolved. First, the equivalent grid impedance model is assumed to be purely inductive, hence, neglecting the effects of the grid resistance on the power losses. Second, estimating the grid inductance relies on the continuous broadband disturbance (PRBS) injected by the inverter, which is unnecessary. Finally, most importantly, this technique is implemented into a grid-connected inverter operating only in the current mode. In summary, there is a need to address the above key problems related to active and reactive control schemes for grid-connected droop-based inverters, as they permit the operation in both the grid-connected and islanding (voltage control) modes.

The contribution of this paper is twofold. First, an adaptive mechanism based on the influence of the transmission-line impedance is proposed for droop-controlled grid-connected inverters to compensate transmission-line losses, hence, maintaining accurate control of the injected power by the inverters through decoupling the active and reactive power flow. Second, the transmission-line resistance and inductance are estimated online by the inverter itself based on the PQ variations algorithm that required only three samples to perform the estimation. Consequently, prior knowledge of the grid parameters is not required. The proposed control strategy allows:

1) Full decoupling between the active and reactive power flow through the transmission line,
2) Precise control of power factor at the grid-side due to the automated mitigation of the unintended power losses across transmission line resistance and inductance (or any segment of it). Therefore, voltage fluctuations at the PCC caused by the coupling of the active and reactive power injection is avoided,
3) Unrestricted control of the inverter active and reactive power, however, the delivered power to the common AC bus is now equal to the desired inverters' references,
4) Simple implementation and highly reduced computational burden of the online transmission-line impedance estimation algorithm,
5) Finally, the proposed adaptive control scheme is reliable as there is no need for communication links, where it needs only local current and voltage measurements.

The rest of the paper is structured as follows: Section II reviews the power flow and the impacts of transmission line impedance on the power flow direction in grid-connected inverter systems. Section III discusses the proposed adaptive control scheme to decouple power flow. Section IV gives the simulation results. Section V presents hardware-in-the-loop experimental results to verify the feasibility of the proposed control strategy. Finally, conclusions are drawn in Section VI.

II. Impacts of Transmission Line Impedance on Operation of Grid-Connected Inverters

The utility grid can be modeled by the Thevenin model consisting of the equivalent voltage source and equivalent impedance. The upper stream of the utility grid (HV/MV transformer + transmission lines) introduces a very small impedance. In contrast, the MV/ LV transformer, especially with the low power rating, and the LV cables introduce relatively high-impedance (resistance + inductance) values. The effects of such impedance become unneglectable for PV-houses and PV farms, especially those which are located far

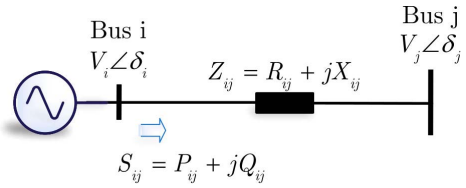

Fig. 2. Simple 2 bus system.

from the common AC feeder such as in remote areas [10]. This impedance causes voltage droop across the feeder when power flows through leading to both active and reactive power losses.

To illustrate further, this section briefly reviews power flow in power systems. Then, the impacts of equivalent transmission-line (grid) impedance on power flow direction between the inverter and grid are elaborated.

A. Power Flow Calculation

Fig. 2 depicts a two bus power system, bus i and bus j. The two buses are connected through a resistive-inductive transmission line. It is worthwhile to mention that the resistive-inductive model is chosen in this paper as it is sufficient to accurately represent the grid impedance at the fundamental frequency (50 Hz) [18], [19], which is the frequency of interest in this paper.

In the system shown in Fig. 2, the apparent power flows from bus i and bus j is expressed by [20]:

$$S_{ij} = V_i e^{j\delta_i}\left(\frac{V_i e^{j\delta_i} - V_j e^{j\delta_i}}{R_{ij} + jX_{ij}}\right)^*, \tag{1}$$

where $V_i e^{j\delta_i}$ and $V_j e^{j\delta_j}$ are the complex voltages of bus i and bus j, respectively. V_i and V_j are the voltages magnitude at bus i and bus j, respectively. δ_i and δ_j are voltages angles of the two buses. In this paper, the upper-case letters with rightwards arrows above donate complex variables, upper-case letters indicate RMS while lower-case letters are used for instantaneous variables. In Fig. 2, the real and reactive power drawing from bus i and flowing to bus j are given by [21]:

$$P_{ij} = V_i^2 G_{ij} - V_i V_j\left(G_{ij}\cos\delta_{ij} + B_{ij}\sin\delta_{ij}\right), \tag{2}$$

$$Q_{ij} = V_i^2 B_{ij} - V_i V_j\left(B_{ij}\cos\delta_{ij} + G_{ij}\sin\delta_{ij}\right), \tag{3}$$

where P_i and Q_i denote the net power injection of active and reactive power at bus i. $\delta_{ij} = \delta_i - \delta_j$ is the angle difference between the voltages of bus i and bus j, respectively. G_{ij} and B_{ij} are the conductance and susceptance between buses i and j, respectively, and calculated by

$$G_{ij} - jB_{ij} = \frac{1}{R_{ij} + jX_{ij}}. \tag{4}$$

Then, the real and reactive power losses in transmission line $i-j$ are given as [22]:

$$P_{loss-ij} = G_{ij}\left(V_i^2 - 2V_i V_j\cos\delta_{ij} + V_j^2\right), \tag{5}$$

$$Q_{loss-ij} = B_{ij}\left(V_i^2 - 2V_i V_j\cos\delta_{ij} + V_j^2\right). \tag{6}$$

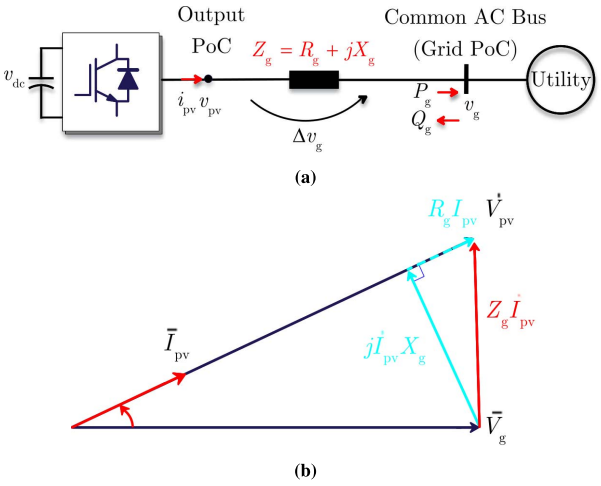

Fig. 3. PV inverter is operated at unity power factor: (a) Block diagram of the system, (b) Phasor diagram of the voltages.

The effects of these active and reactive power losses on the power flow from the grid-connected inverter systems to the grid are explain in the next subsection.

B. Impacts of Transmission Line Impedance on Power Flow Direction in Grid-Connected Inverter Systems

To illustrate the negative impact of transmission line impedance on power flow direction and associated losses, a typical three-phase PV inverter system operating in the grid-connected mode is shown in Fig. 3a is considered. v_{pv} is the voltage at the inverter side (Output PoC), i_{pv} is the current injected to the grid by the PV inverter, v_g and Z_g equivalent grid voltage and grid impedance. R_g and L_g are equivalent grid resistance and inductance ($\mathbf{Z}_g = R_g + jX_g = |Z_g|\angle\theta_g$). The phasor diagram of the voltages when the inverter is operated at the unity power factor is shown in Fig. 3b, where $\vec{I}_{pv}$, $\vec{V}_{pv}$ and $\vec{V}_g$ are the phasors of i_{pv}, v_{pv}, and v_g, respectively. Based on Fig. 3b, the inverter operation can be expressed using the root-mean-square (RMS) values as [17]:

$$V_{pv} = \sqrt{V_g^2 - \left(X_g I_{pv}\right)^2} + R_g I_{pv}. \tag{7}$$

Eq. (5), (6), and (7) show that the transmission line impedance poses several challenges that prevent accurate control of the power flow. As mentioned earlier, the coupling between the active and reactive power flow also results in deterioration of the electricity quality of the common AC bus such as power factor deterioration and voltage flickers under fluctuating renewable power generation. For instance, when the inverter is operating at unity power factor and injecting real power to the grid, the injected current to the grid is leading the grid voltage due to the impact of grid Z_g that causes unintended power losses and reverse reactive power flow from the grid source (Grid PoC) to the transmission line.

Another example of the negative impact of Z_g is when it is desired to enable the inverter to provide support to the grid at a specific location of interest by injecting only a certain amount of real power to a specific bus. However, the delivered power

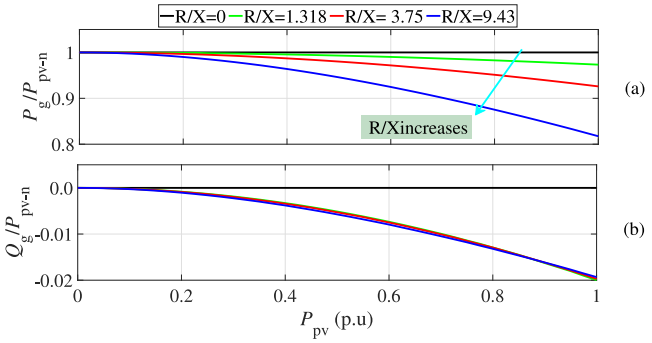

Fig. 4. Negative impacts of grid impedance with different R/X ratios on coupling the delivered power to the grid when an inverter system rated at $P_{pv-n} = 50$ kW is operated at unity power factor: (a) Active power, (b) Reactive power.

from the inverter to this bus (P_g) is less than the desired reference due to the active power losses across the line impedance located between the inverter and this bus. Additionally, the power factor at this bus is decreased due to the reverse reactive power Q_g from the bus (grid) to the inverter side in order to compensate for the reactive power losses across the equivalent line impedance. Fig. 4(a) and Fig. 4(b) show the negative impacts of grid impedance with different R/X ratios [23] on the delivered active and reactive power to the grid when a 50 kW inverter system is operated at unity power factor. This decoupling and losses become a major concern in weak grids and for high power rating inverter systems (e.g., PV/wind farms), as the introduced coupling minimizes the inverter's capability to maintain the desired power factors at the grid side (Grid PoC) or any segment of the transmission line.

Hence, in the following, an adaptive mechanism that addresses the aforementioned shortcomings is proposed, which does not need any extra hardware, requires only local measurements, and is implemented into droop-controlled grid-connected inverters.

III. Proposed Adaptive Power Control

The proposed adaptive power control strategy is shown in Fig. 5 and Fig. 6. The inverter is interfaced to the grid via an LCL filter. The proposed method is consisting of two stages: 1) estimating the transmission line impedance (referred interchangeably as grid impedance), and 2) online calculation of the adaptive terms required for compensation line losses and decouple both the active and reactive power across the estimated grid. It is worth mentioning that that that the proposed control relies on decoupling both the active and reactive power flow, while it still permitting unrestricted control of the active and reactive power commands provided to the inverter by, for example, the dispatch center.

A. Online Estimation of Grid Impedance and Voltage Using Droop-Based Grid-Connected Inverters

The first step to realize the proposed control is to obtain the information of the transmission line impedance that is desired to control the power flow through. Here, two different approaches can be adopted. First, if the impedance information is known during the design stage, the adaptive power control could be programmed accordingly. This approach is preferable if it is required to decouple the power flow through a specific segment of the transmission line. Second, if the impedance information is unknown and the aim is to decouple the power flow through the entire transmission line, it is possible to enable the inverter to estimate the grid impedance online. This approach is practical as the grid impedance is a time-varying parameter, also the estimation could be performed without additional hardware. The second approach that relies on the local online impedance estimation by the inverter is explained in the rest of this subsection.

In this paper, the PQ variations technique is proposed for the droop-based grid-connected inverter. This estimation technique is embedded into the control loop of the inverter. It is simple, accurate, and it enables the estimation of both the grid resistance and inductance. The followed method of the PQ variations technique is explained briefly below.

Fig. 7(a) illustrates the working principle of how the impedance estimation using PQ variations works [24]. $\vec{V}_{pcc1}$, $\vec{I}_{pcc1}$, $\vec{V}_{pcc2}$ and $\vec{I}_{pcc2}$ are the phasor representation of the voltage and current measurements at the PCC of the inverter at two different operating points (e.g., 1 and 2). Z_g is the phasor representations of the unknown grid impedance. As the $\vec{V}_g$ is immeasurable, the main idea of estimating Z_g is to intentionally enforce the inverter to work in different operating points (e.g., 1 and 2) throughout deliberate variations in the output active and reactive power, as presented in Fig. 7(a) in order to avoid the unknown variable $\vec{V}_g$. The equations describing the inverter in these two operation points are given by:

$$\begin{cases} \vec{V}_{pcc1} = \vec{I}_{pcc1} Z_g + \vec{V}_g, & \text{(8a)} \\ \vec{V}_{pcc2} = \vec{I}_{pcc2} Z_g + \vec{V}_g. & \text{(8b)} \end{cases}$$

By subtracting (8b) from (8a), the unknown variable $\vec{V}_g$ is avoided. Then, Z_g can be calculated online as follows:

$$Z_g = R_g + jX_g = \frac{\vec{V}_{pcc1} - \vec{V}_{pcc2}}{\vec{I}_{pcc1} - \vec{I}_{pcc2}} = \frac{\Delta \vec{V}_{pcc12}}{\Delta \vec{I}_{pcc12}}. \quad (9)$$

It is worth mentioning that the PQ variations strategy can be based on two, three, or four operation points. In this paper, the method based on three operating points, as illustrated in Fig. 7(b), is used as it minimizes the inherent coupling in the dq reference frame [25].

To enable the impedance estimation, a trigger command is activated. Then, the three operating points are obtained. The first operating point ($\vec{V}_{pcc1}$ and $\vec{I}_{pcc1}$) is obtained from the steady-state conditions of the system at Δt_1. However, the second operating point ($\vec{V}_{pcc2}$ and $\vec{I}_{pcc2}$) is obtained by varying the active power ΔP for a specific time Δt_2. Recalling (9), the equivalent grid resistance R_g is extrapolated based on the filtered dq voltage and current measurements (V_{dq} and I_{dq}) as follows:

$$R_g = \Re\left[\frac{\Delta \vec{V}_{pcc12}}{\Delta \vec{I}_{pcc12}}\right] = \frac{\Delta V_{d12}\Delta I_{d12} + \Delta V_{q12}\Delta I_{q12}}{\Delta {I_{d12}}^2 + \Delta {I_{q12}}^2}. \quad (10)$$

Finally, the third operating point (V_{pcc3} and I_{pcc3}) is obtained from varying the reactive power ΔQ for a specific time Δt_3. Similarly, the equivalent grid reactance X_g is

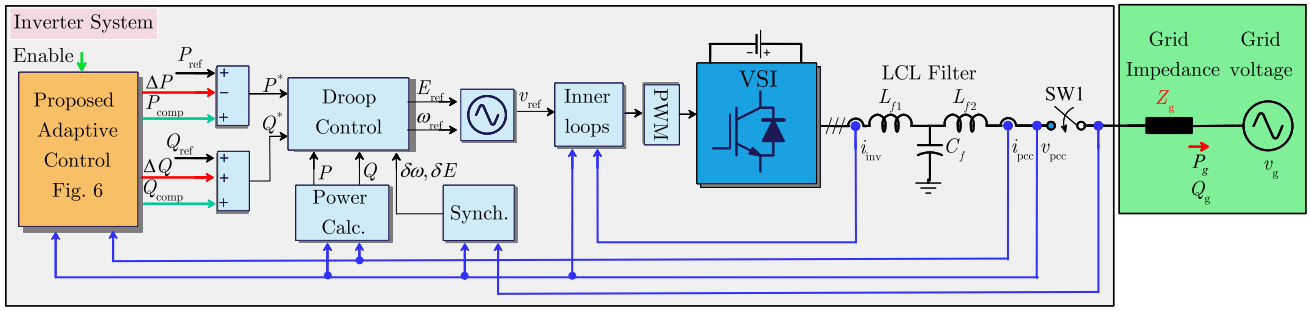

Fig. 5. Schematic diagram of the investigated inverter system with the proposed adaptive control scheme for accurate active and reactive power flow. P_{comp} and Q_{comp} are the adaptive terms for compensating the losses (and decoupling power flow), and ΔP, ΔQ are the required power variations for grid impedance estimation.

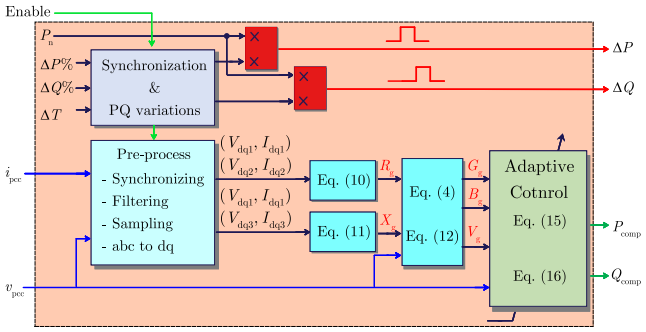

Fig. 6. Proposed adaptive power control scheme including online grid impedance estimation.

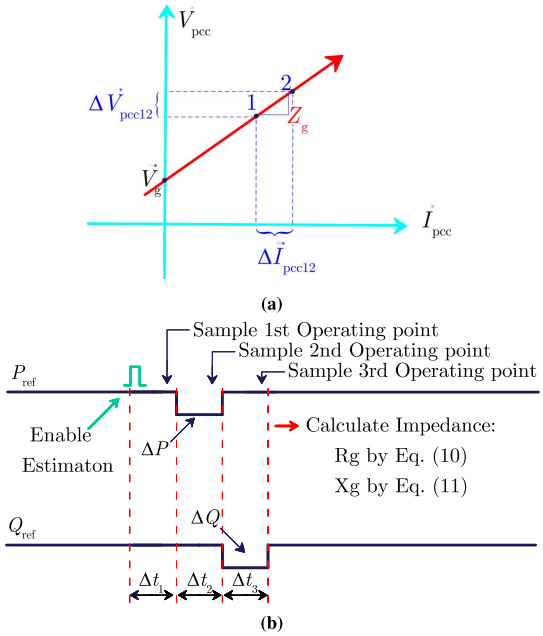

Fig. 7. (a) V -I characteristic of the grid when the power converter working in two operation points at a particular frequency, (b) Impedance estimation using PQ variations based on obtaining three operating points [19], [25].

calculated as follows:

$$X_{\text{g}} = \Im\left[\frac{\Delta\vec{V}_{\text{pcc13}}}{\Delta\vec{I}_{\text{pcc13}}}\right] = \frac{\Delta V_{\text{q13}}\Delta I_{\text{d13}} - \Delta V_{\text{d13}}\Delta I_{\text{q13}}}{\Delta I_{\text{d13}}{}^2 + \Delta I_{\text{q13}}{}^2}. \quad (11)$$

In addition, the unknown grid voltage $\vec{V}_{\text{g}}$ can now be estimated from the measurement of the PCC voltage and current phasors and based on the estimated impedance in (10) and (11) as follows:

$$\vec{V}_{\text{g}} = \vec{V}_{\text{pcc}} - \vec{I}_{\text{pcc}} Z_{\text{g}}. \quad (12)$$

The proposed methodology to estimate the grid parameters has the advantage of avoiding unnecessary periodic PQ variations [24], [25], [26], [27] since it will be activated only once a trigger command is received.

B. Adaptive Control of Active and Reactive Power Flow

The proposed control strategy is based on modifying the active and reactive power references of the frequency and voltage droop loops, respectively. It considers the effects of both the transmission line resistance and inductance components on the power flow between the inverter and the grid.

Once the grid impedance is estimated as shown above, the adaptive control is activated. The control laws proposed for the droop-control grid connected inverter are given as follows:

$$P^* = P_{\text{ref}} - \Delta P + P_{\text{comp}}, \quad (13)$$

$$Q^* = Q_{\text{ref}} + \Delta Q + Q_{\text{comp}}, \quad (14)$$

where P^* and Q^* are the modified power references for the droop control. P_{ref} and Q_{ref} are the desired power references. ΔP and ΔQ are the proposed terms to perform the required power variations to estimate the grid impedance components (resistance and inductance). P_{comp} and P_{comp} are the proposed adaptive terms to compensate both the active and reactive power losses across the transmission line resistance and inductance. These two terms also ensure the flow of active power through the distribution lines will not cause unintended reverse reactive power flow from the grid-side and vice versa with the reactive power flow while persevering unrestricted control of the inverter output active and reactive power. However, the delivered power to the common AC bus (the grid-side) is now equal to the power reference commands (P_{ref} and Q_{ref}).

Recalling (5) and (6), and by considering power flow laws in 3-phase system, the power losses ($P_{\text{loss-pcc,g}}$, $Q_{\text{loss-pcc,g}}$) across the grid impedance due to injected current by the inverter can be adaptively calculated by the inverter itself based on 1) the estimated grid impedance components ($R_{\text{g}}, L_{\text{g}}, G_{\text{g}}, B_{\text{g}}$), 2) the estimated grid voltage $\vec{V}_{\text{g}} = V_{\text{g}}\angle\delta_{\text{g}}$, and 3) the instantaneous output measurements of the inverter. Now, P_{comp} and Q_{comp} terms in (13) and (14) are set to

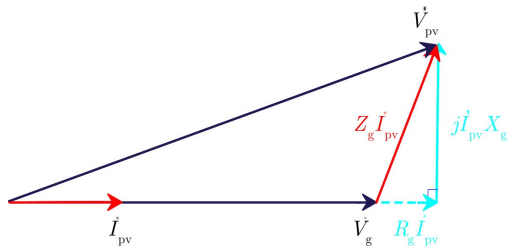

Fig. 8. Phasor diagram of the voltages when the inverter system shown in Fig. 3 is operating at unity power factor under the proposed control.

$P_{\text{loss-pcc,g}}$ and $Q_{\text{loss-pcc,g}}$. Finally, the compensation terms are given by:

$$P_{\text{comp}} = 3G_{\text{g}}\Big(V_{\text{pcc}}^2 - 2V_{\text{pcc}}V_{\text{g}}\cos\big(\delta_{\text{pcc}} - \delta_{\text{g}}\big) + V_{\text{g}}^2\Big), \quad (15)$$

$$Q_{\text{comp}} = 3B_{\text{g}}\Big(V_{\text{pcc}}^2 - 2V_{\text{pcc}}V_{\text{g}}\cos\big(\delta_{\text{pcc}} - \delta_{\text{g}}\big) + V_{\text{g}}^2\Big), \quad (16)$$

where δ_{pcc} and δ_{g} are the angles of the PCC voltage and the estimated grid voltage.

To not lose generality, the proposed terms (15) and (16) can also be used to compensate the power losses across a specific segment of the transmission line in order to enable accurate control of the power flow between the inverter and this location of interest. To do so, the impedance of this segment of the transmission line should be known first, either from the online impedance estimation or from the design specifications, in order to be used in the control loop shown in Fig. 6. Then, the voltage at the location of interest is calculated based on (12). Finally, the compensation terms are being calculated in real-time by (15) and (16) and used to modify the inverter power reference commands according to (13) and (14), respectively.

Fig. 8 shows the phasor diagram of the network voltages after enabling the proposed control scheme for the inverter operating in unity power factor, and considering power flow decoupling for the entire transmission line. The effects of the equivalent grid impedance are fully mitigated through the adaptive compensation terms. In contrast, the current injected into the grid is lagging the grid voltage source under the conventional droop control due to the equivalent grid impedance, as shown in Fig. 3b.

IV. Simulation Results

To evaluate the performance of the proposed control strategy, the system of Fig. 3 is simulated in MATLAB/Simulink using the Simscape electrical library and PLECS blockset. The corresponding values of the system parameters are listed in Table I. Three sets of tests are conducted to verify 1) power loss compensation for the entire transmission line impedance, including verifying the accuracy of the transmission line impedance estimation based on the PQ variations algorithm that is embedded into the droop control, 2) power loss compensation for a specific segment of the transmission line, and in the presence of another inverter connected to the common AC bus, and 3) the accuracy of the impedance estimation in the presence of local load at the inverter PCC.

TABLE I
Simulation Parameters of the System

Description	Symbol	Value	Unit
Grid parameters			
Grid line-to-neutral voltage (RMS)	V_{g}	230	V
Grid frequency	f_{g}	50	Hz
Equivalent grid impedance	R_{g}	60	$m\Omega$
	L_{g}	300	μH
Inverter parameters			
Inverter nominal power	P_n	350	kW
Frequency droop gain	m_p	1.79^{-5}	rad/sec/W
Voltage droop gain	n_p	9.29^{-5}	V/Var
Impedance estimation algorithm			
Required estimation time	T_{est}	1.5	sec
Active power variations	ΔP	10.5 (3%)	kW
Reactive power variations	ΔQ	10.5 (3%)	kVar

A. Power Loss Compensation for the Entire Transmission Line Impedance

In this part, the real value of the transmission line resistance and inductance are $R_{\text{g}} = 60\ m\Omega$ and $L_{\text{g}} = 300\mu$H. The inverter is initially operating in a steady-state under the conventional droop control and power reference commands are $P_{\text{ref}} = 300$ kW and $Q_{\text{ref}} = 0$ kVar. At $t = 3$ sec, the impedance estimation algorithm is enabled.

Then, required PQ variations starts at 3.5 sec, where $\Delta P = 3\%P_n$ is subtracted from the inverter's active power reference ($P_{\text{ref}} - \Delta P$) from 3.5 sec to 4.0 sec. Afterwards, the $\Delta Q = 3\%P_n$ is added to the reactive power reference ($Q_{\text{ref}} + \Delta Q$) from 4.0 sec to 4.5 sec. It can be observed that the total required time for impedance estimation is 1.5 sec, from 3.0 to 4.5 sec. This relatively long time is chosen to ensure accurate sampling of the three operation points after the inverter reaches steady-state operation during PQ variations. This is an important factor in the estimation as droop-based inverters are characterized by their slower time response compared to current source inverters.

Fig. 9a and Fig. 9b compare the online estimation results of the equivalent grid resistance and inductance with real (donated by ref) values listed in Table. I. It is evident that the estimation algorithm provides very accurate estimation results. The errors in the estimated resistance R_{g} and inductance L_{g} components are $\Delta R_{\text{g}} = -0.67\%$ and $\Delta L_{\text{g}} = 0.33\%$.

Fig. 10a shows that the instantaneous active P_{g} and reactive Q_{g} power at the grid side. Before $t = 6$ sec, P_{g} and Q_{g} power are less than their desired references because of the power losses across the transmission line impedance. However, enabling the proposed method for $t \geq 6$ sec allows adaptive compensation of these losses while permitting full control of active and reactive power, separately; see the reactive power change to $Q_{\text{ref}} = 50$ kVar from 8 sec. Hence, the grid impedance impacts on control of the active and reactive power are fully mitigated, and the delivered active and reactive power to the grid side are now controlled independently.

Fig. 10b shows P_{comp} and Q_{comp} terms that are being calculated in real-time from (15) and (16). Between 6 and 8 sec, these values are 34.1 kW and 53.4 kVar, respectively. Then, they increase slightly for t $\geq$ 8 sec, following the step increase in the inverter reactive power command.

Fig. 11 shows the inverter's apparent power, where enabling the proposed power control strategy (P_{comp} and Q_{comp}) causes

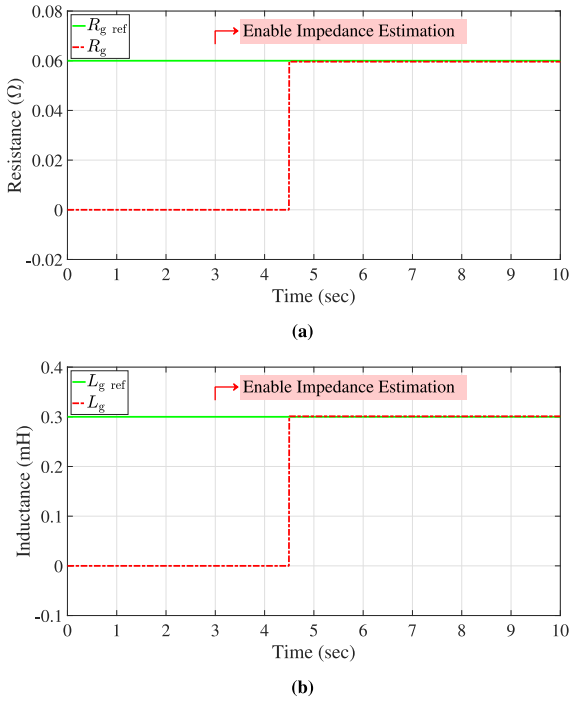

Fig. 9. The real and online estimated components of the equivalent grid impedance seen by the inverter: (a) Grid resistance, (b) Grid inductance.

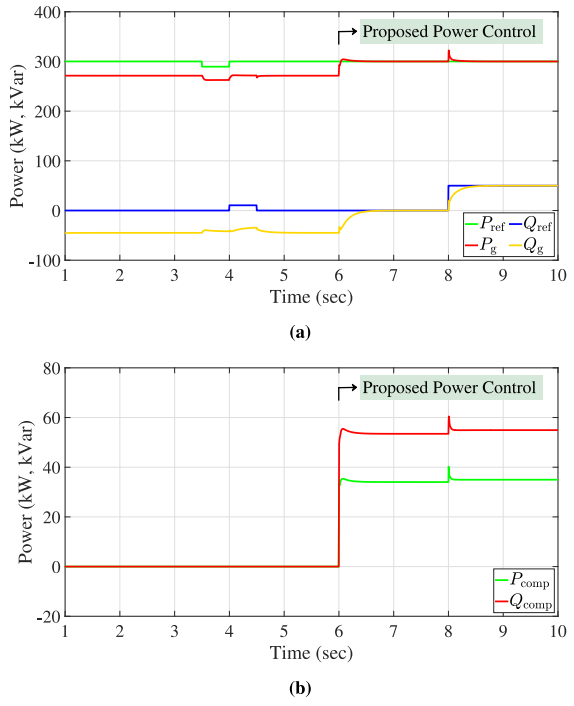

Fig. 10. (a) Active and reactive power waveforms, (b) adaptive power terms to compensate grid impedance losses.

an increase in the inverter output power in order to decouple the active and reactive power at the grid side. Fig. 11 shows also an overshoot in the apparent power occurs at 8 sec. This is due to the step change in the reactive power reference of the inverter that leads voltage fluctuations. To solve this, a ramp increase instead of a sharp step-change of the power reference commands can be applied, as recommended by standards.

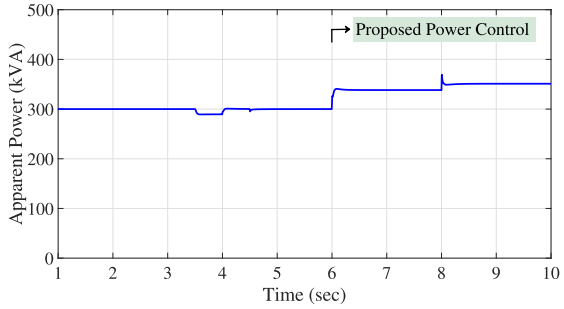

Fig. 11. Apparent power of the inverter.

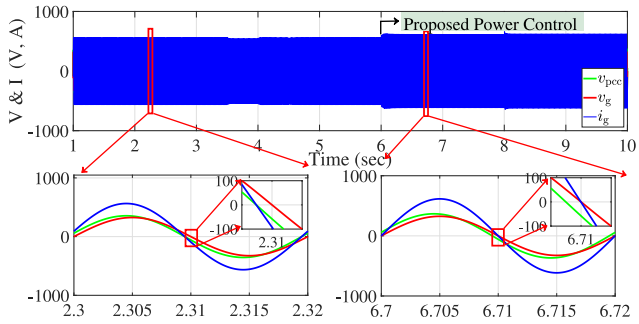

Fig. 12. Voltage and current waveforms.

Fig. 12 shows the voltages and current waveforms. Under the conventional technique, the phase of the inverter output current (denoted by i_g) is not identical to the grid voltage. This phase difference is related to the equivalent grid impedance seen by the inverter. However, these waveforms maintained the same phase under the proposed control scheme that is enabled from 6 sec.

B. Power Loss Compensation for a Specific Segment of the Transmission Line and in the Presence of Other Inverters

To test the effectiveness of the proposed power loss compensation for a specific segment of the transmission line (feeder 1), and in the presence of other inverters in the network, the test system shown in Fig. 13(a) is considered. The corresponding values of the system parameters are identical to Table I. Additionally, the impedance values of feeder 1 and 2 are set to $R_{f1} = R_{f1} = 30\ m\Omega$ and $L_{f1} = L_{f1} = 150\mu$H. The proposed power control scheme is embedded here only for inverter 1 to compensate/decouple power of feeder 1.

Fig. 13(b) shows the power reference commands for inverter 1 and the delivered P_1 and Q_1 power by the inverter to the common AC bus. P_{comp} and Q_{comp} are being calculated in this case based on (15) and (16), respectively. However, R_{f1} and L_{f1} are being used instead of R_g and R_g. Fig. 13(c) depicts voltage and current waveforms for this test in which the phases of the inverter current and the voltage of the common AC bus grid voltage v_{bus} are identical only after the proposed control scheme is enabled at 6.0 sec.

This case study shows how the propose control strategy is fixable, and it can be employed to enable smart droop-based inverters to deliver accurate amount of active and reactive power to a desired location (here the common AC bus), which

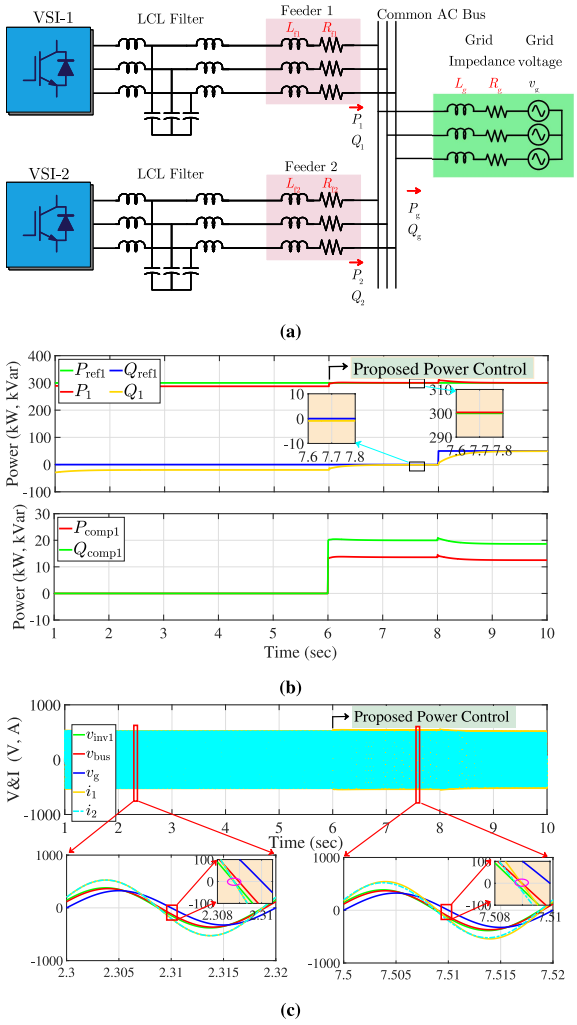

Fig. 13. Control of P_1 and Q_1 by compensation of power loss across the specific segment of the transmission line (feeder 1): (a) System configuration of the two identical parallel droop-based inverters, (b) Reference commands and delivered active and reactive power by inverter 1 to the common AC bus, and the adaptive power terms for inverter 1 to compensate power loss across feeder 1, (c) Voltage and current waveforms.

is beneficial for potential ancillary services applications such as frequency and voltage support.

C. Estimation of Equivalent Grid Impedance in the Presence of Local Load

In this section the accuracy of the grid impedance estimation is tested in the presence of local load. Fig. 14(a) shows the network topology used for the investigation. It consists of the droop-based inverter, local active load $P_{\text{load}} = 10$ kW, and grid Thevenin model.

Fig. 14(b) shows the online estimation results ($R_{\text{eq,est}}$, $L_{\text{eq,est}}$) of equivalent impedance seen by the inverter. It can be observed that the estimated grid impedance components are very close to those results obtained without the presence of local load, as shown earlier in Fig. 9. This is true as the equivalent reference impedance seen by the inverter (Z_{eq}) is the parallel connection of Z_{g} and Z_{load}, where Z_{load} is the impedance of the local load (here $Z_{\text{load}} = R_{\text{load}} = 15.87\Omega$ at 10 kW and 230 V). Hence, where the real value in the presence of the local load is $Z_{\text{g}}//R_{\text{load}} = 0.0603 + 2.977 \times 10^{-4}$s.

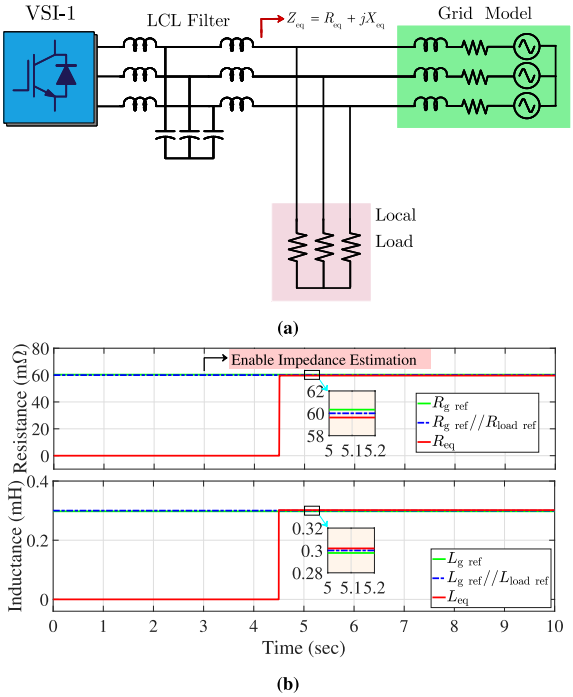

Fig. 14. Estimation of the equivalent grid impedance in the presence of a 50 kW local load: (a) System configuration, (b) The real and estimated impedance components by the inverter.

It can be noticed that the value of the grid impedance dominates the equivalent impedance at the frequency of interest (50 Hz) [19]. In other words, it can be written that $Z_{\text{eq}}(50\text{ Hz}) \approx Z_{\text{g}}(50\text{ Hz})$. In summary, this test indicates the small impact of the presence of local loads that are connected to the PCC on the estimation accuracy of the equivalent grid impedance. The effect will become further minimal for small power rating load due to its equivalent parallel high impedance.

V. Experimental Results

To further verify the feasibility of the proposed control strategy, Hardware-in-the-loop (HIL) experimental results are presented for the three-phase droop-based grid-connected inverter shown in Fig. 5. Also, the system parameters are identical to those listed in Tab. I.

Fig. 15 shows the realization of the experiment platform. The power stage of the three-phase 350 kW inverter is implemented into RT Box CE from Plexim GmbH, while the control algorithm is realized through a DSP LAUNCHXL-F28069M from Texas Instruments. PLECS software is used for programming and real-time interfacing of both RT Box CE and the DSP card. The corresponding current, voltage, and power waveforms are exported by digital-to-analog converters to be displayed on a Tektronix oscilloscope.

Two cases are reported to test the performance of the proposed control while the inverter operates at unity and non-unity power factor, respectively.

A. Operation Under Unity Power Factor

In this case study, the reference power commands of the inverter are set to $P_{\text{ref}} = 300$ kW and $Q_{\text{ref}} = 0$ kVar. Then, the proposed control is activated to regulate the grid-side power (P_{g} and Q_{g}) to their desired reference commands.

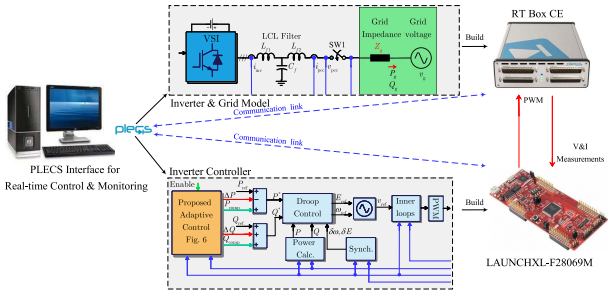

(a)

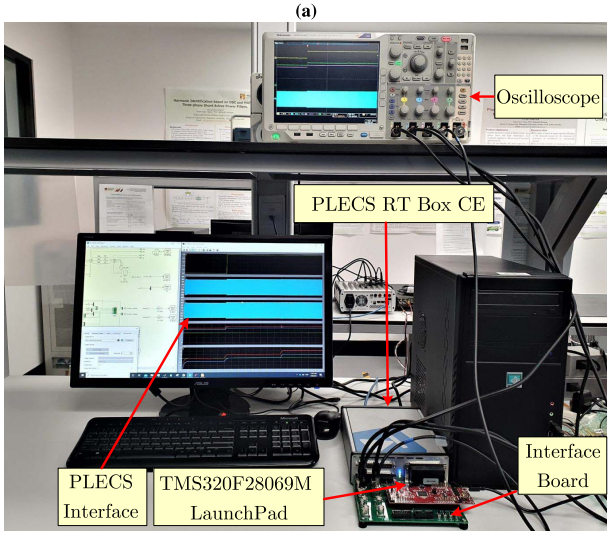

(b)

Fig. 15. Hardware-in-the-Loop testbed: (a) block diagram of the system, (b) photograph of the testbed.

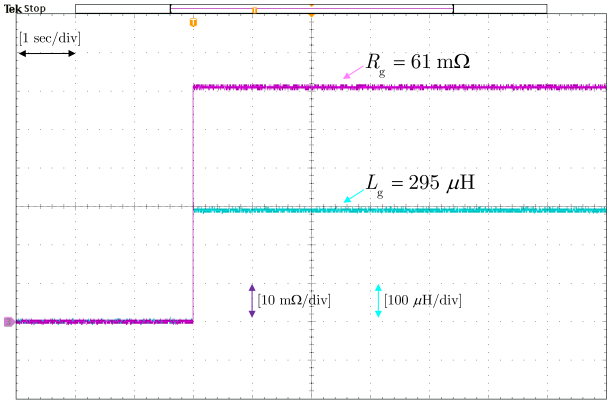

Fig. 16. Online estimation of the equivalent grid impedances by the droop-based inverter.

Fig. 16 shows the online estimation of the grid resistance and inductance by the inverter. It is evident that the estimation algorithm provides very close estimation results to the real values, where the errors in the estimated resistance and inductance components are $\Delta R_g = 1.67\%$ and $\Delta L_g = -1.6\%$, respectively.

Fig. 17 shows the experimental power and current waveforms before and after enabling the adaptive power control. On the one hand, it can be seen that the delivered power to the grid under the conventional droop control is 271 kW and −45 kVar due to the effects of the grid impedance. On the other hand, the values of P_g and Q_g are regulated to the desired references after enabling the proposed control scheme. Fig. 17 shows also the expected slight increase in the inverter output current under the proposed power control.

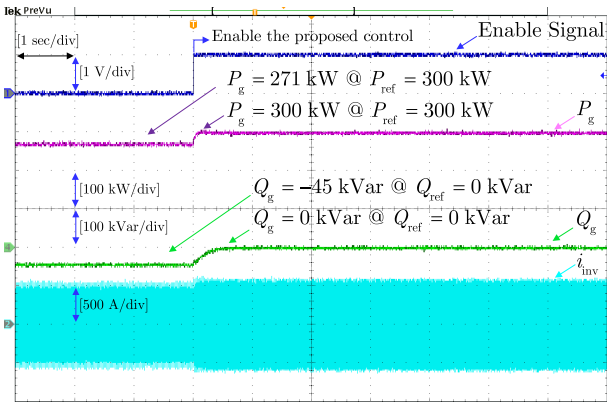

Fig. 17. Waveforms of the delivered power to the grid and the inverter output current in case of unity power factor operation under the conventional and the proposed droop control schemes.

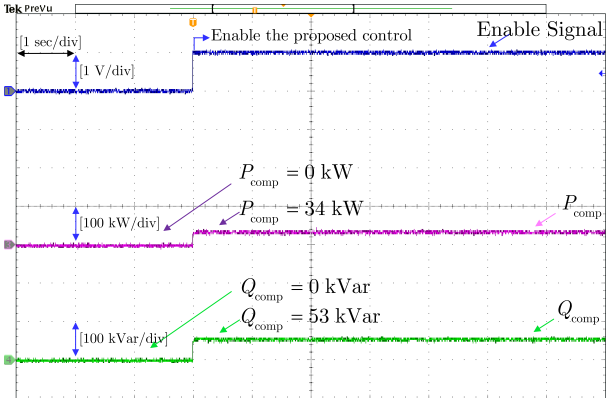

Fig. 18. Enabling signal and the proposed adaptive power terms P_{comp}, Q_{comp} to mitigate the grid impedance effects.

Fig. 18 shows the adaptive active and reactive power (P_{comp} and Q_{comp}) of the inverter. The injected power by the proposed control strategy allows the full decoupling of the active and reactive power at the grid side. For example, the reverse reactive power flow of −45 kVar presented in Fig. 17 is now avoided, which is in accordance with the aim, theoretical analysis and simulation results.

Fig. 19a and Fig. 19b show the current and voltage waveforms of the system before and after enabling the proposed control, respectively. It can be seen that the phase angles of the inverter output current (i_{inv}) the grid voltage (v_g) are identical only after enabling the proposed control.

B. Operation Under Non-Unity Power Factor

To verify the fact that the proposed control permits independent control of active and reactive power, a step change in the reactive power command Q_{ref} the inverter from 0 kVar to 50 kVar is applied, while the active power command is kept constant at $P_{ref} = 300$ kW.

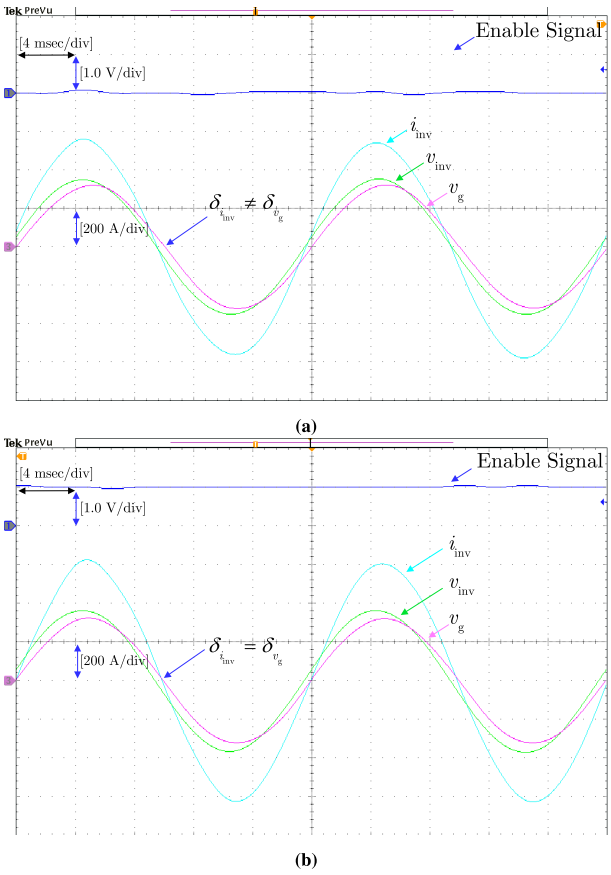

Fig. 19. Current and voltage waveforms of the system at unity power factor: (a) with the conventional droop control, (b) After enabling the proposed control.

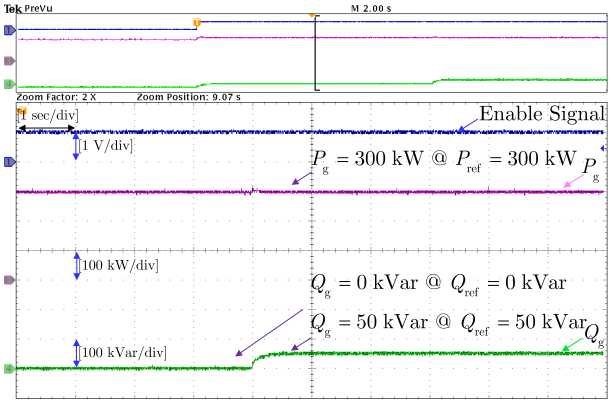

Fig. 20. Waveforms of the delivered power to the grid during applying a step change in the reactive power reference from 0 kVar to 50 kVar under the proposed droop control scheme.

Fig. 20 shows the power waveforms. It can be observed that the adaptive power control algorithm ensures accurate control of the desired active and reactive power independently. As stated previously, the full decoupling of active and reactive power flow is accomplished in real-time based on the instantaneous local measurements and the information of grid impedance.

Fig. 21 depicts the current and voltage waveforms of the system while the proposed control is enabled. It can be seen that the phase angle of the inverter output current is lagging

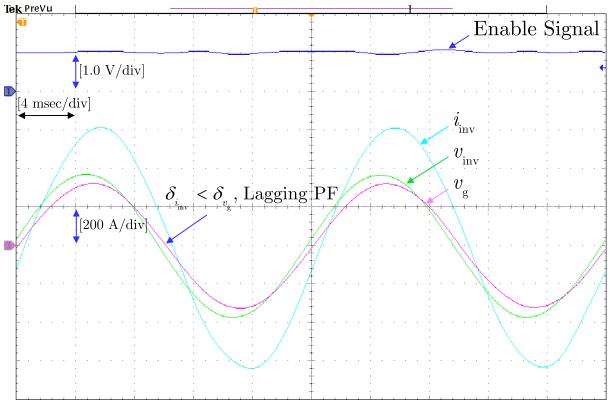

Fig. 21. Current and voltage waveforms under the proposed control at a non-unity power factor, where $Q_{ref} = 50$ kVar.

from the phase angle of the grid voltage, $\delta_{i_{inv}} < \delta_{v_g}$, indicating lagging power factor due to injection of positive reactive power.

VI. Conclusion

This paper proposes an adaptive power control for droop-controlled grid-connected inverters in order to leverage the potential benefits for seamless operation and control of grid forming inverters in grid-connected mode. This control strategy allows real-time and automated decoupling of the active and reactive power flow by compensating the unintended active and reactive power loss through the equivalent transmission line impedance (or a segment of it) seen by the inverter at its PCC. The proposed technique consists of two stages. First, an online impedance estimation technique is embedded into the control loop. Afterwards, the estimated impedance components (resistance and inductance) are utilized to calculate the amount of the active and reactive power required to adaptively compensate the power losses across the network impedance (or a part of it) for a given inverter output instantaneous current. Both the required PQ variations to estimate the transmission line resistance and inductance and the adaptive terms to compensated impedance losses are added on top of the power reference commands. Hence, precise control of the injected power/power factor at the grid-side (or at the end of a specific segment of the transmission line) are ensured while persevering unrestricted control of the inverter active and reactive power commands. Simulation and hardware-in-the-loop experimental results of a three-phase 350 kW inverter system are provided to validate the effectiveness of the proposed scheme, which has potential applications related to inverter-based grid support services (e.g., voltage/frequency support) using smart grid forming inverters.

References

[1] B. K. Bose, "Power electronics, smart grid, and renewable energy systems," *Proc. IEEE*, vol. 105, no. 11, pp. 2011–2018, Nov. 2017

[2] K. Turitsyn, P. Sulc, S. Backhaus, and M. Chertkov, "Options for control of reactive power by distributed photovoltaic generators," *Proc. IEEE*, vol. 99, no. 6, pp. 1063–1073, Jun. 2011.

[3] T. F. Guerin, "Impacts and opportunities from large-scale solar photovoltaic (PV) electricity generation on agricultural production," *Environ. Qual. Manag.*, vol. 28, no. 4, pp. 7–14, 2019.
[4] P. Chiradeja, "Benefit of distributed generation: A line loss reduction analysis," in *Proc. IEEE/PES Transm. Distrib. Conf. Exposit. Asia–Pacific*, Dalian, China, 2005, pp. 1–5.
[5] M. J. Parajeles, R. Ramirez, and G. Valverde, "Use of smart inverters for provision of voltage support to medium and high voltage networks," in *Proc. IEEE 2nd Global Power Energy Commun. Conf. (GPECOM)*, Izmir, Turkey, 2020, pp. 291–296.
[6] N. Sockeel, J. Gafford, B. Papari, and M. Mazzola, "Virtual inertia emulator-based model predictive control for grid frequency regulation considering high penetration of inverter-based energy storage system," *IEEE Trans. Sustain. Energy*, vol. 11, no. 4, pp. 2932–2939, Oct. 2020.
[7] F. Ding and M. Baggu, "Coordinated use of smart inverters with legacy voltage regulating devices in distribution systems with high distributed PV penetration—Increase CVR energy savings," *IEEE Trans. Smart Grid*, early access, Jul. 18, 2018.
[8] R. Seguin, J. Woyak, D. Costyk, J. Hambrick, and B. Mather, "High-penetration PV integration handbook for distribution engineers," NREL, Golden, CO, USA, NERL Rep. NREL/TP-5D00-63114, 2016.
[9] R. K. Varma and M. Akbari, "Simultaneous Fast Frequency Control and Power Oscillation Damping by Utilizing PV Solar System as PV-STATCOM," *IEEE Trans. Sustain. Energy*, vol. 11, no. 1, pp. 415–425, Jan. 2020.
[10] M. Liserre, R. Teodorescu, and F. Blaabjerg, "Stability of photovoltaic and wind turbine grid-connected inverters for a large set of grid impedance values," *IEEE Trans. Power Electron.*, vol. 21, no. 1, pp. 263–272, Jan. 2006.
[11] C. Wan, M. Huang, C. K. Tse, and X. Ruan, "Effects of interaction of power converters coupled via power grid: A design-oriented study," *IEEE Trans. Power Electron.*, vol. 30, no. 7, pp. 3589–3600, Jul. 2015.
[12] Y. Song, X. Wang, and F. Blaabjerg, "Impedance-based high-frequency resonance analysis of DFIG system in weak grids," *IEEE Trans. Power Electron.*, vol. 32, no. 5, pp. 3536–3548, May 2017.
[13] Y. Li, S. Liu, J. Zhu, X. Yuan, Z. Xu, and K. Jia, "Novel MTDC droop scheme with decoupled power control for enhancing frequency stabilities of weak AC systems," *IET Renew. Power Gener.*, vol. 14, no. 11, pp. 2007–2016, Aug. 2020.
[14] H. Alenius, R. Luhtala, T. Messo, and T. Roinila, "Autonomous reactive power support for smart photovoltaic inverter based on real-time grid-impedance measurements of a weak grid," *Elect. Power Syst. Res.*, vol. 182, May 2020, Art. no. 106207.
[15] J. M. Guerrero, J. C. Vasquez, J. Matas, L. G. De Vicuna, and M. Castilla, "Hierarchical control of droop-controlled AC and DC microgrids—A general approach toward standardization," *IEEE Trans. Ind. Electron.*, vol. 58, no. 1, pp. 158–172, Jan. 2011.
[16] G. Liu, X. Cao, W. Wang, T. Ma, W. Yang, and Y. Chen, "Adaptive control strategy to enhance penetration of PV power generations in weak grid," in *Proc. Int. Power Electron. Appl. Conf. Exposit.*, Shanghai, China, 2014, pp. 1217–1221.
[17] D. Yang, X. Wang, F. Liu, K. Xin, Y. Liu, and F. Blaabjerg, "Adaptive reactive power control of PV power plants for improved power transfer capability under ultra-weak grid conditions," *IEEE Trans. Smart Grid*, vol. 10, no. 2, pp. 1269–1279, Mar. 2019.
[18] R. Rosso, J. Cassoli, G. Buticchi, S. Engelken, and M. Liserre, "Robust stability analysis of *LCL* filter based synchronverter under different grid conditions," *IEEE Trans. Power Electron.*, vol. 34, no. 6, pp. 5842–5853, Jun. 2019.
[19] N. Mohammed, T. Kerekes, and M. Ciobotaru, "An online event-based grid impedance estimation technique using grid-connected inverters," *IEEE Trans. Power Electron.*, vol. 36, no. 5, pp. 6106–6117, May 2021.
[20] H. Saadat, *Power System Analysis*. Boston, MA, USA: McGraw-Hill, 1999.
[21] Z. Yang, H. Zhong, A. Bose, T. Zheng, Q. Xia, and C. Kang, "A linearized OPF model with reactive power and voltage magnitude: A pathway to improve the MW-only DC OPF,"İ *IEEE Trans. Power Syst.*, vol. 33, no. 2, pp. 1734–1745, Mar. 2018.
[22] R. Cordero, "Estimation of transmission losses in a changing electric power industry," M.S. thesis, Dept. Elect. Eng. Comput. Sci., Massachusetts Inst. Technol., Cambridge, MA, USA, 1996.
[23] N. Mohammed, M. Ciobotaru, and G. Town, "Fundamental grid impedance estimation using grid-connected inverters: A comparison of two frequency-based estimation techniques," *IET Power Electron.*, vol. 13, no. 13, pp. 2730–2741, 2020.
[24] M. Ciobotaru, R. Teodorescu, P. Rodriguez, A. Timbus, and F. Blaabjerg, "Online grid impedance estimation for single-phase grid-connected systems using PQ variations," in *Proc. Rec. IEEE Annu. Power Electron. Spec. Conf. (PESC)*, Orlando, FL, USA, 2007, pp. 2306–2312.
[25] N. Mohammed, M. Ciobotaru, and G. Town, "An improved grid impedance estimation technique under unbalanced voltage conditions," in *Proc. IEEE PES Innov. Smart Grid Technol. Eur. (ISGT-Europe)*, Bucharest, Romania, 2019, pp. 1–5.
[26] A. V. Timbus, P. Rodriguez, R. Teodorescu, and M. Ciobotaru, "Line impedance estimation using active and reactive power variations," in *Proc. IEEE Power Electron. Spec. Conf.*, Orlando, FL, USA, 2007, pp. 1273–1279.
[27] A. V. Timbus, R. Teodorescu, and P. Rodriguez, "Grid impedance identification based on active power variations and grid voltage control," in *Proc. IEEE Ind. Appl. Annu. Meeting*, vol. 1. New Orleans, LA, USA, 2007, pp. 949–954.

Nabil Mohammed (Member, IEEE) received the bachelor's degree (Hons.) in electrical power engineering from Tishreen University in 2013, the M.Eng. (Mechatronics and Automatic Control) degree from Universiti Teknologi Malaysia in 2017, and the Ph.D. degree in power electronics from Macquarie University, Australia, in 2021.

During the summer of 2019, he was a Visiting Researcher with the Department of Energy Technology, Aalborg University, Denmark. He is currently a Postdoctoral Research Fellow with Monash University, Australia. His research interests include power electronics converters, renewable energy generation and integration in power systems, microgrids, energy storage and management systems, and adaptive control.

Mihai Ciobotaru (Senior Member, IEEE) received the Eng. Diploma and M.Eng. degrees in electrical engineering from the University of Galati, Galati, Romania, in 2002 and 2003, respectively, and the Ph.D. degree in electrical engineering from Aalborg University, Aalborg, Denmark, in 2009.

He continued with the University of Galati as an Associate Lecturer until 2004 and with Aalborg University as an Associate Research Fellow until 2010. He joined the University of New South Wales, Sydney, NSW, Australia, as a Research Fellow, where he continued as a Senior Research Fellow until 2018. Thereafter, he joined Macquarie University, Sydney, as a Senior Lecturer with the School of Engineering. He is currently an Adjunct Fellow with Macquarie University and a Principal Engineer with EcoJoule Energy. His main research activities and interests include power electronic inverters, power management of hybrid energy storage systems, module-level power electronics for photovoltaic systems, and dc distribution networks for more electric aircrafts.